

REPORT DOCUMENTATION PAGE

Form Approved
OMB No. 0704-0188

Public reporting burden for this collection of information is estimated to average 1 hour per response, including the time for reviewing instructions, searching existing data sources, gathering and maintaining the data needed, and completing and reviewing this collection of information. Send comments regarding this burden estimate or any other aspect of this collection of information, including suggestions for reducing this burden to Department of Defense, Washington Headquarters Services, Directorate for Information Operations and Reports (0704-0188), 1215 Jefferson Davis Highway, Suite 1204, Arlington, VA 22202-4302. Respondents should be aware that notwithstanding any other provision of law, no person shall be subject to any penalty for failing to comply with a collection of information if it does not display a currently valid OMB control number. **PLEASE DO NOT RETURN YOUR FORM TO THE ABOVE ADDRESS.**

1. REPORT DATE (DD-MM-YYYY) 14-05-2007		2. REPORT TYPE Conference Paper (Preprint)		3. DATES COVERED (From - To) May 2007 - May 2007	
4. TITLE AND SUBTITLE Pulsed Injection Flow Control for Throttling in Supersonic Nozzles – A Computational Fluid Dynamics Based Performance Correlation (Preprint)				5a. CONTRACT NUMBER	
				5b. GRANT NUMBER	
				5c. PROGRAM ELEMENT NUMBER	
6. AUTHOR(S) Neal D. Domel, Dan Baruzzini and Daniel N. Miller				5d. PROJECT NUMBER DARPO52Z	
				5e. TASK NUMBER	
				5f. WORK UNIT NUMBER	
7. PERFORMING ORGANIZATION NAME(S) AND ADDRESS(ES) Lockheed Martin Aeronautics Company Propulsion Systems and CFD Technologies Post Office Box 748, Mail Zone 9333 Fort Worth, TX 76101				8. PERFORMING ORGANIZATION REPORT NUMBER AFRL-PR-ED-TP-2007-277	
9. SPONSORING / MONITORING AGENCY NAME(S) AND ADDRESS(ES) Air Force Research Laboratory (AFMC) AFRL/PRS 5 Pollux Drive Edwards AFB CA 93524-7048				10. SPONSOR/MONITOR'S ACRONYM(S)	
				11. SPONSOR/MONITOR'S NUMBER(S) AFRL-PR-ED-TP-2007-277	
12. DISTRIBUTION / AVAILABILITY STATEMENT Distribution A: Approved for public release; distribution unlimited (PA # 07199A).					
13. SUPPLEMENTARY NOTES For presentation at the 37 th AIAA Fluid Dynamics Conference, Miami, FL, 25-28 Jun 2007. Paper No. AIAA-2007-4214.					
14. ABSTRACT A vehicle propelled by an engine with a variable geometry nozzle allows the nozzle expansion ratio to vary with altitude and flight condition, thereby optimizing vehicle performance. Rockets are examples of vehicles with high nozzle pressure ratios (NPR's), which operate over a large altitude range. Active flow control offers a method of reducing the effective aerodynamic throat of a rocket nozzle in a geometrically fixed structure. Throttling the mass flow rate through the nozzle throat controls the effective throat area, subsequently controlling the effective expansion ratio of the overall nozzle. This paper presents findings from the Pulsed Injection for Rocket Flow Control Technology (PIRFCT) program, which was funded by the Defense Advanced Research Projects Agency (DARPA), and managed by the Air Force Research Laboratory (AFRL). PIRFCT evaluated potential gains in the overall performance of a rocket using active flow control at the throat for throttling. Lockheed Martin Aeronautics Company used Computational Fluid Dynamics (CFD) to simulate a high NPR rocket nozzle with active flow control. Simulations were performed with steady and pulsed flow control jets which were oriented near the throat and directed upstream at a 45 degree angle against the primary flow, and various injection conditions were modeled. All simulations were performed with the perfect gas assumption with the specific heat ratio (γ) held constant at the value corresponding to the throat temperature. However, during the course of the program, a correlation was developed which predicts the reduction in discharge coefficient as a function of time-averaged mass flux, momentum flux and energy flux. The correlation was very general and was valid for steady and pulsed cases of various conditions. This correlation proved to be useful in determining steady injection cases which were equivalent to pulsed injection cases. Simulations of the equivalent steady cases were much less computationally intensive than the pulsed cases. This paper focuses on the basic scientific and engineering process and the resulting throttling correlation. The effect of throat injection on exit thrust is also discussed. The PIRFCT program concluded that a typical rocket is not a good candidate for this type of throttling technology because of the small portion of its trajectory spent at lower altitudes where back-pressure changes are significant.					
15. SUBJECT TERMS					
16. SECURITY CLASSIFICATION OF:			17. LIMITATION OF ABSTRACT SAR	18. NUMBER OF PAGES 16	19a. NAME OF RESPONSIBLE PERSON 1Lt Jannette J. Cohen
a. REPORT Unclassified	b. ABSTRACT Unclassified	c. THIS PAGE Unclassified			19b. TELEPHONE NUMBER (include area code) N/A

Pulsed Injection Flow Control for Throttling in Supersonic Nozzles – A Computational Fluid Dynamics Based Performance Correlation (Preprint)

Neal D. Domel¹, Dan Baruzzini² and Daniel N. Miller³
Lockheed Martin Aeronautics Company, Propulsion Systems and CFD technologies, Post Office Box 748, Fort Worth, Texas, 76101, Mail Zone 9333

A vehicle propelled by an engine with a variable geometry nozzle allows the nozzle expansion ratio to vary with altitude and flight condition, thereby optimizing vehicle performance. Rockets are examples of vehicles with high nozzle pressure ratios (NPR's), which operate over a large altitude range. Active flow control offers a method of reducing the effective aerodynamic throat of a rocket nozzle in a geometrically fixed structure. Throttling the mass flow rate through the nozzle throat controls the effective throat area, subsequently controlling the effective expansion ratio of the overall nozzle. This paper presents findings from the Pulsed Injection for Rocket Flow Control Technology (PIRFCT) program, which was funded by the Defense Advanced Research Projects Agency (DARPA), and managed by the Air Force Research Laboratory (AFRL). PIRFCT evaluated potential gains in the overall performance of a rocket using active flow control at the throat for throttling. Lockheed Martin Aeronautics Company used Computational Fluid Dynamics (CFD) to simulate a high NPR rocket nozzle with active flow control. Simulations were performed with steady and pulsed flow control jets which were oriented near the throat and directed upstream at a 45 degree angle against the primary flow, and various injection conditions were modeled. All simulations were performed with the perfect gas assumption with the specific heat ratio (γ) held constant at the value corresponding to the throat temperature. However, during the course of the program, a correlation was developed which predicts the reduction in discharge coefficient as a function of time-averaged mass flux, momentum flux and energy flux. The correlation was very general and was valid for steady and pulsed cases of various conditions. This correlation proved to be useful in determining steady injection cases which were equivalent to pulsed injection cases. Simulations of the equivalent steady cases were much less computationally intensive than the pulsed cases. This paper focuses on the basic scientific and engineering process and the resulting throttling correlation. The effect of throat injection on exit thrust is also discussed. The PIRFCT program concluded that a typical rocket is not a good candidate for this type of throttling technology because of the small portion of its trajectory spent at lower altitudes where back-pressure changes are significant.

¹ Aeronautical Engineer Senior Staff, Propulsion Integration, AIAA Lifetime Senior Member.

² Aeronautical Engineering Staff, Propulsion Integration, AIAA Member.

³ Principal Engineer, Lockheed Martin Fellow, Vehicle Sciences & Systems, AIAA Associate Fellow.

Distribution A: Approved for public release; distribution unlimited.

Copy right © 2007 by Lockheed Martin Aeronautics. All rights reserved. Published by American Institute of Aeronautics and Astronautics, Inc. with permission

Nomenclature

A	Area	P_t	Stagnation pressure
a	Slope of linear correlation	p	Static pressure
C_d	Discharge coefficient	St	Strouhal number, $f\left(\frac{w}{V_{inj}}\right)$
C_{d_0}	Baseline C_d (no injection)	T	Static Temperature
C_p	Specific heat at constant pressure	T_t	Stagnation Temperature
C_v	Specific heat at constant volume	V	Velocity
d	Diameter	V_{\perp}	Normal Velocity Component
f	Frequency of pulsing	w	injector slot width
f	Injected momentum flux	x	Independent variable
F	Primary momentum flux	ρ	Density
H	Stagnation Enthalpy	γ	Ratio of specific heats, $\frac{c_p}{c_v}$
I_{sp}	Vacuum specific impulse	τ	T_t ratio, $\frac{(T_t)_{inj}}{(T_t)_{pri}}$
M	Mach number	ω	\dot{m} ratio, $\frac{\dot{m}_{inj}}{\dot{m}_{pri}}$
\dot{m}	Mass flux		
$\dot{m}H$	Energy flux		
R	Specific gas constant		

Subscripts

inj	Injected flow quantity
pri	Primary flow quantity
ref	Reference quantity
0	Baseline property (no injection)

I. Introduction

Traditionally, rocket engines have been designed with a fixed geometry nozzle which optimizes the expansion ratio for an atmospheric pressure which corresponds to a specific altitude. However, the actual atmospheric pressure decreases during ascent; therefore, a rocket engine with constant post-combustion stagnation conditions would need to continuously change its expansion ratio in order to optimize thrust for all ambient pressures. The complexity and expense of a variable geometry nozzle has generally been cost prohibitive for rocket engines, which are often intended for one use only.

The Air Force Research Laboratory (AFRL), with funding from the Defense Advanced Research Projects Agency (DARPA), tasked a team of three companies to investigate the viability of using active flow control to change the effective aerodynamic throat of the nozzle. With this technique, the nozzle exit would remain fixed, but the effective throat area would be reduced, thereby increasing the expansion ratio of the nozzle. Figure 1 shows a generic nozzle with secondary flow being injected near the throat to create enough blockage that the effective throat is significantly smaller than the geometric throat.

Lockheed Martin's role was to simulate the nozzle with Computational Fluid Dynamics (CFD) for steady and pulsed injection and provide injection requirements to achieve the desired amount of throttling. The other contractors determined the overall system tradeoffs, and investigated the possibility of developing the hardware to deliver the required properties (e.g., steady redirected flow, high frequency pulsing pumps, etc.) Lockheed Martin has significant experience in flow control simulation and technology development involving steady and pulsing jets, as well as passive forms of flow control such as vanes and ramps (Catt et al., 1995, Miller et al., 1995, 1997, 2001), (Vakili, 1999), (Yagle et al., 2000, 2002).

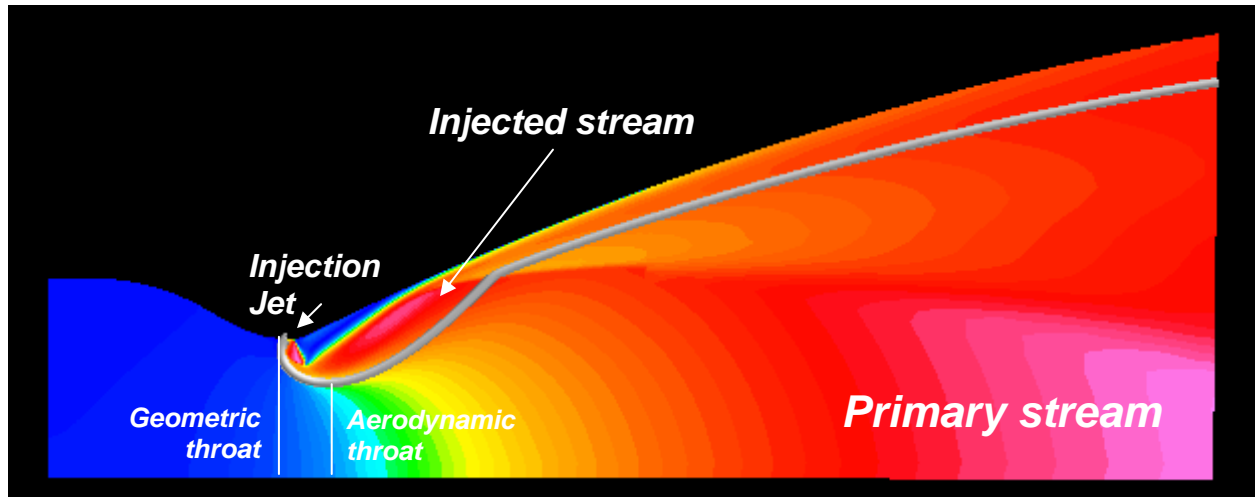


Figure 1. Generic Nozzle with throat injection

II. CFD Methodology

Lockheed Martin's FALCON CFD code was used to perform the required simulations. The code uses a structured-grid, multi-block topology, with compressible finite volume discretization. Turbulence is modeled with the option of a Reynolds-Averaged Navier-Stokes (RANS) or Large Eddy Simulation (LES). The code uses implicit solvers and has a parallel solver capability. The code is used extensively in the analysis of air vehicle flows.

FALCON uses the upwind flux difference splitting of Roe (1981) for the convective terms. This discretization uses second or third order MUSCL (van Leer, 1976) extrapolation of the fluxes with the option of flux limiting using the MINMOD (Roe, 1981) or SUPERBEE (Sweby, 1984) limiters. For time accurate solutions, FALCON uses a second-order, three point backward difference of the time term. Viscous fluxes are discretized using second-order central differences.

Two implicit solvers are available, a symmetric Gauss-Seidel (SGS) method and the Strongly Implicit Procedure (SIP) of Stone (1968). For unsteady solutions, a dual time stepping approach is used where the solution is iterated at each time step to convergence using one of the solvers. The implicit solvers allow for rapid convergence of the solution at each time step. This approach removes CFL restrictions resulting from fine grid spacing near no-slip walls, thereby requiring fewer iterations for an unsteady solution.

FALCON uses a 2-equation k - ϵ turbulence model with optional wall functions for RANS simulations (Smith, 1990), and an algebraic stress model to relate the turbulent stresses to the strain rate. For simulations requiring resolution of small time scales (below the appropriate range for RANS), the turbulence is modeled based on the LES formulation of Smagorinsky (1963) and extended to include compressibility effects. Wall functions are used to increase the allowable normal spacing near a solid wall.

The present investigation relied primarily upon RANS simulations for steady injection cases, and LES for pulsed cases. For the scope of this study, the simulations were performed with the perfect gas assumption. Although the simulated stagnation temperatures are around 6000 degrees Rankine, high temperature real gas effects are not modeled, with the exception that the ratio of specific heats, γ , was set to a constant value of 1.1296. This value approximates the exhaust products in the primary nozzle throat. The pulsing frequencies for this study ranged from about 5000Hz to about 63000Hz. This range was chosen in order to cluster our data points about a Strouhal number of 0.3, which was a value favored by a previous study.

The high frequencies and high injection Mach numbers required the development of a compressible pulse boundary condition which is described in the next section.

III. Compressible Pulse Boundary Condition

A perfect square wave is the computational standard for the time history of a simulated pulsing jet. However, early attempts at simulations revealed challenges to numerical stability and robustness for an injection jet

instantaneously switching between zero and supersonic flow at the frequencies of interest. Therefore, each wave cycle was separated into segments in which 5 states modeled a physics-based transition between the “on” and “off” conditions. This approach uses classic characteristic unsteady 1-D relations (Anderson, 1982). Figure 2 illustrates the profile of injection Mach, pressure and mass flux during a single cycle. Rather than the jet instantly turning “on” and remaining constant at a specified supersonic condition for half the cycle, a brief duration of sonic injection initiates the cycle. This sonic condition defines state 1. This initial sonic condition mimics what realistically happens when the exit of a pressurized stagnant diverging injector nozzle is suddenly exposed to a sufficiently low back pressure. The duration of the sonic conditions is set to an estimate of the time required by acoustic waves to travel upstream to the injector throat and then return to the exit. (Only the injector exit is present in the CFD simulation. It is flush with the main nozzle surface such that the same grid may be used to simulate the geometry with no injector.) These waves are part of the transient process which then allow the exit conditions to accelerate to the steady state supersonic Mach number dictated by steady quasi-1D relations. The sonic condition persists until state 2, which designates the moment when the flow begins to expand from sonic to the specified supersonic condition (state 3) according to the inward running (from the boundary into the computational domain) unsteady 1-D characteristic relation. The jet conditions remain constant at state 3 during the majority of the “on” portion of the cycle until state 4, which designates the moment when the jet begins to turn “off.” The flow then expands to Mach 0 (state 5) according to the outward running unsteady 1-D characteristic relation. The characteristic relations are shown below, where velocity, V , is positive directed from the boundary into the computational domain (injector aligned).

$$\text{inward running characteristic : } V + \frac{2}{\gamma - 1} \sqrt{\gamma RT} = \text{constant}$$

$$\text{outward running characteristic : } V - \frac{2}{\gamma - 1} \sqrt{\gamma RT} = \text{constant}$$

Conditions during the “off” portion of the cycle are defined by the interior conditions and zero flow assumption at the boundary (similar to a no-slip wall). The wall pressure is calculated from the pressure, acoustic speed and normal velocity component at the first interior point according to the inward running characteristic relation, where V is the normal component of velocity measured as positive into the computational domain. The time duration from states 1 to 2, 2 to 3, and 4 to 5 require assumptions about the effective length of the injector nozzle. This length is chosen is such that the accumulated time spent during these intermediate phases is generally less than 10% that of the ideal “on” portion of the cycle. This allows a finite number of numerical time-steps to occur during these rapid changes. The time-average mass, momentum and energy flux closely approximates that of a perfect square wave, but the numerical robustness is dramatically improved and allows the number of time steps per wave to be a few hundred. This was necessary for the timely simulation of the large rocket nozzle with a high frequency injector pulsing with a Mach 2 square wave and a stagnation pressure approximately six times that of the primary flow.

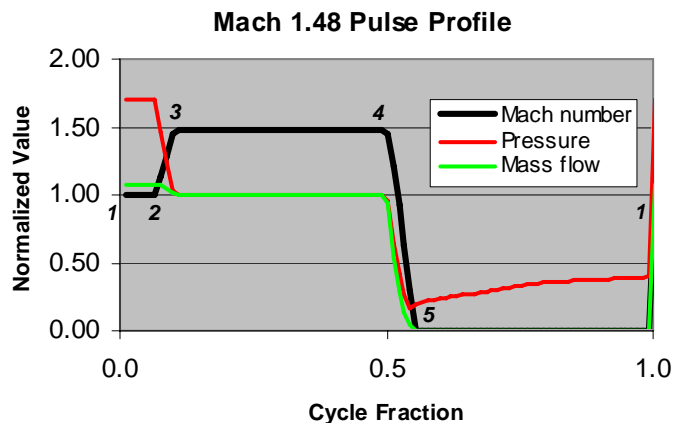


Figure 2. Modified Square Wave for Compressible Pulse Boundary Condition

This modification to a square wave addresses the computational issues, but the practical difficulty of designing a test article to behave this way at high frequencies remains a challenge for the experimentalist.

IV. Correlation for Throttling

A. Equivalent Steady Injection

This paper is dedicated to describing the approach used for comparing steady and pulsed injection, and defining a simple correlation which is valid for predicting the amount of throttling for either steady or pulsed injection. A companion paper compares the various simulations in more detail.

Because of the large amounts of computer resources required for time-accurate simulations of rocket nozzles with pulsing injectors, a method was needed to predict the throttling performance of a pulsed (or steady) injector without simulating each case with CFD. The basis for comparing pulsed and steady injectors was decided to be the time-averaged fluxes of mass, momentum and energy. For a given pulsed case, all three time-averaged fluxes may be obtained by time-averaging the CFD solution. An “equivalent steady” case is then defined as one which steadily injects the time-averaged fluxes of the pulsing case. Any difference between the performance of a pulsed case and the equivalent steady case would help isolate the benefit/effect of pulsing. The formulas for the three fluxes are shown below with \dot{m} and H expanded. These formulas are valid for the primary nozzle flow or the secondary injector flow. (The momentum flux is designated as F and f for the primary nozzle and secondary injector, respectively. Also, the momentum equation contains a reference pressure, p_{ref} , which is the pressure at the sonic condition in the primary nozzle throat, and is described further in a later section.)

$$\text{mass flux :} \quad \dot{m} = A\{\rho V\}$$

$$\text{momentum flux (} F \text{ or } f \text{):} \quad \dot{m}V + (p - p_{ref})A = A\{\rho V^2 + (p - p_{ref})\}$$

$$\text{energy flux :} \quad \dot{m}H = A\rho V c_p T_t = A\left\{\frac{1}{2}\rho V^3 + \rho V c_p T\right\}$$

The nearly ideal square-wave profiles of the simulated injected fluxes allow for easy time-averaging because each flux may be approximated as a constant value during the “on” portion of the cycle, and then zero during the “off” portion. Therefore, each time-averaged flux may be estimated from the “on” condition, the injector area, and the duty cycle. For a known set of “on” conditions, the area varies inversely with the duty cycle to produce the same time-averaged fluxes. In other words, a pulsed injector square-wave with a 50% duty cycle produces the same time-averaged fluxes as an “equivalent steady” injector (100% duty cycle) with half the injector area with the same “on” conditions. Similarly, a square wave pulsing with a 25% duty cycle would have an equivalent steady case whose jet has $\frac{1}{4}$ the area of the pulsing case, but with the same velocity and thermodynamic properties as the “on” portion of the pulsed case. This concept is mathematically simple, but the subtle difference between it and conventional correlations is the involvement of all three fluxes, each of which scales linearly and consistently with jet area.

B. Injected Fluxes

The fluxes have been formulated above to show that A_{inj} may be factored and isolated out of all three fluxes, but V_{inj} may *not* be factored and isolated in a similar manner. The exponent which appears on V_{inj} varies from zero to three in the various terms in the flux formulations. Therefore, the fluxes will not scale consistently with velocity. However, all fluxes scale consistently with area. This area scaling is the key to sizing an equivalent steady injector which matches the three time-averaged fluxes of an injector pulsing with a square wave profile. (Scaling with density would be possible if p_{ref} scaled with injection density. However, p_{ref} is defined as the pressure where the primary fluxes are calculated; therefore, it is not dependent upon injection density.)

C. Primary Fluxes

The fluxes of the primary flow are calculated from the stagnation conditions, which are applied at the inflow boundary, and the mass flux, which is measured at the inflow boundary. The pulsing of the injector jet causes pressure waves to travel upstream to the inflow boundary, thereby causing fluctuations in the primary mass flow and static properties at the inflow boundary. However, these fluctuations are usually small and regular, and allow a time averaged mass flow to be readily obtained. The measured mass flow and the applied stagnation temperature allow the primary mass and energy fluxes to be calculated at the inflow. Time-averaged mass and energy fluxes are assumed to remain constant as they expand through the nozzle. The momentum flux is derived from the additional assumption that the stagnation condition expands isentropically to Mach 1 at the nozzle throat, which defines the

primary velocity and the reference pressure, p_{ref} , where the primary momentum flux is calculated. This calculation is shown below. Here, the unsubscripted variables refer to primary conditions.

$$\begin{aligned}
 \text{primary momentum flux : } F &= \dot{m}V + (p - p_{ref})A \\
 &= \dot{m}M\sqrt{\gamma RT} + (p - p_{ref})A \\
 &= \dot{m}M\sqrt{\frac{\gamma RT_t}{1 + \frac{\gamma-1}{2}M^2}} + (p - p_{ref})A \\
 &= \dot{m}\sqrt{\frac{2\gamma}{\gamma+1}RT_t} \text{ where } M = 1 \text{ and } p = p_{ref} = p_{t_{pri}}\left(\frac{2}{\gamma+1}\right)^{\frac{\gamma}{\gamma-1}}
 \end{aligned}$$

D. Combined Flux Function

Because of the difficulty in varying one flux without varying the other two, a function was defined which combines all three fluxes into a single independent variable such that comparisons of discharge coefficients could be made among cases with injected flows of different pressures, temperatures, Mach numbers, etc.. Several combinations of the fluxes were attempted, but the following ‘‘combined flux function’’ emerged as a good flux function which allowed the discharge coefficients to collapse onto a single curve.

$$\text{combined flux function : } x = \sqrt{\frac{f}{F} \sqrt{\frac{\dot{m}_{inj}}{\dot{m}_{pri}} \frac{(\dot{m}H)_{inj}}{(\dot{m}H)_{pri}}}} \quad \text{and } a = 5.6 \text{ (for the PIRFCT geometry)}$$

The combined flux function formula for x reduces to $x = \frac{f}{F}$ when the mass and energy flux ratios scale directly with the momentum flux ratio. This would be true for a set of cases in which τ does not change and which are nearly perfectly expanded (i.e., $p_{inj} \approx p_{ref}$). This momentum flux ratio is the familiar form from previous investigations (Catt, 1995, Miller, 1995).

Further reformulation of the combined flux function shows that it is also closely related to $\omega\sqrt{\tau}$ for an equivalent steady injection case. The term, $\omega\sqrt{\tau}$, is another familiar combination from previous investigations (Catt, 1995). The ‘‘ K ’’ term contains effect of M_{inj} and $p_{inj} - p_{ref}$ (or $\frac{P_{inj}}{P_{pri}}$). $K = 1$ for perfectly expanded sonic injection ($p_{inj} = p_{ref}$ and $M_{inj} = 1$). (In this study, the injection conditions cause $\dot{m}_{inj}V_{inj} \gg |p_{inj} - p_{ref}|A_{inj}$. Therefore, high levels of under/over-expansion were not simulated.) The plot of K in figure 3 shows that a low $\frac{P_{inj}}{P_{pri}}$ combined with a high M_{inj} reduces K , which is detrimental. However, a high $\frac{P_{inj}}{P_{pri}}$ yields diminishing returns when $p_{inj} - p_{ref}$ becomes large.

$$\begin{aligned}
 x &= \sqrt{\frac{f}{F} \sqrt{\frac{\dot{m}_{inj}}{\dot{m}_{pri}} \frac{(\dot{m}H)_{inj}}{(\dot{m}H)_{pri}}}} = \omega\sqrt{\tau}K \quad \text{where : } K = \sqrt{\frac{\gamma+1}{2} \left(\frac{M_{inj}}{\sqrt{1 + \frac{\gamma-1}{2}M_{inj}^2}} + \frac{(p_{inj} - p_{ref})A_{inj}}{\dot{m}_{inj}\sqrt{\gamma RT_{inj}}} \right)} \\
 \text{or : } K &= \sqrt{\frac{\gamma+1}{2} \frac{M_{inj}}{\sqrt{1 + \frac{\gamma-1}{2}M_{inj}^2}} \left\{ 1 + \frac{1}{\gamma M_{inj}^2} \left[1 - \frac{P_{t_{pri}}}{P_{t_{inj}}} \left(\frac{1 + \frac{\gamma-1}{2}M_{inj}^2}{\frac{\gamma+1}{2}} \right)^{\frac{\gamma}{\gamma-1}} \right] \right\}}
 \end{aligned}$$

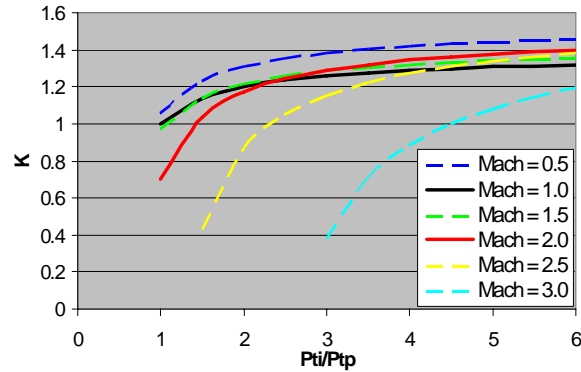


Figure 3. The coefficient of $\omega\sqrt{\tau}$ approaches a Mach-dependent asymptote

E. PIRFCT Correlation

A derived curve-fit was based on an equation which monotonically decreased as the combined flux function increased. The PIRFCT correlation is based upon the combined flux function:

$$\text{PIRFCT correlation : } c_d = \frac{c_{d_0}}{\sqrt{1+ax}} \quad \text{where } x = \text{combined flux function} = \sqrt{\frac{f}{F} \sqrt{\frac{\dot{m}_{inj} (\dot{m}H)_{inj}}{\dot{m}_{pri} (\dot{m}H)_{pri}}}}$$

Figure 4 plots the results of several CFD simulations against each of the 3 fluxes as well as the combined flux function (affectionately nicknamed “3-flux combo”). The plotted discharge coefficient, c_d , is normalized by the baseline discharge coefficient, c_{d_0} . Beneath each plot is an accompanying plot where $\frac{c_d}{c_{d_0}}$ is further formulated into $\left(\frac{c_{d_0}}{c_d}\right)^2 - 1$, which should appear linear with slope “a” according to the form of the PIRFCT correlation. Significant scatter is visible in the data when the discharge coefficient is plotted against any of the three basic fluxes. This scatter is expected since the all three fluxes vary among the data points. However, the combined flux function allows a way to predict and compare cases with very different injection properties. The plots contain data points from steady and pulsed simulations with various injection frequencies, temperatures, pressures, Mach numbers, duty cycles, and number of injection streams. The various simulations are described in more detail in a companion paper. Some of the results are for points with minor geometry differences. (The value of “a” in the PIRFCT correlation is expected to vary with primary nozzle geometry and injector position and orientation. However, these results are all plotted together because the differences are minor.)

The comparison plots show that the blockage produced by a pulsed injector may be predicted from its equivalent steady case. The dependence upon frequency is very slight. This relationship between pulsing and equivalent steady injection is valid for this application where the discharge coefficient (i.e., blockage/throttling) is the figure of merit. One would expect more dependence upon frequency if the baseline case had a natural “reference” frequency. This equivalent flux correlation was useful for the CFD investigation because it allowed the study to rely heavily upon steady state simulations which are much less computationally intensive than time-accurate pulsing simulations.

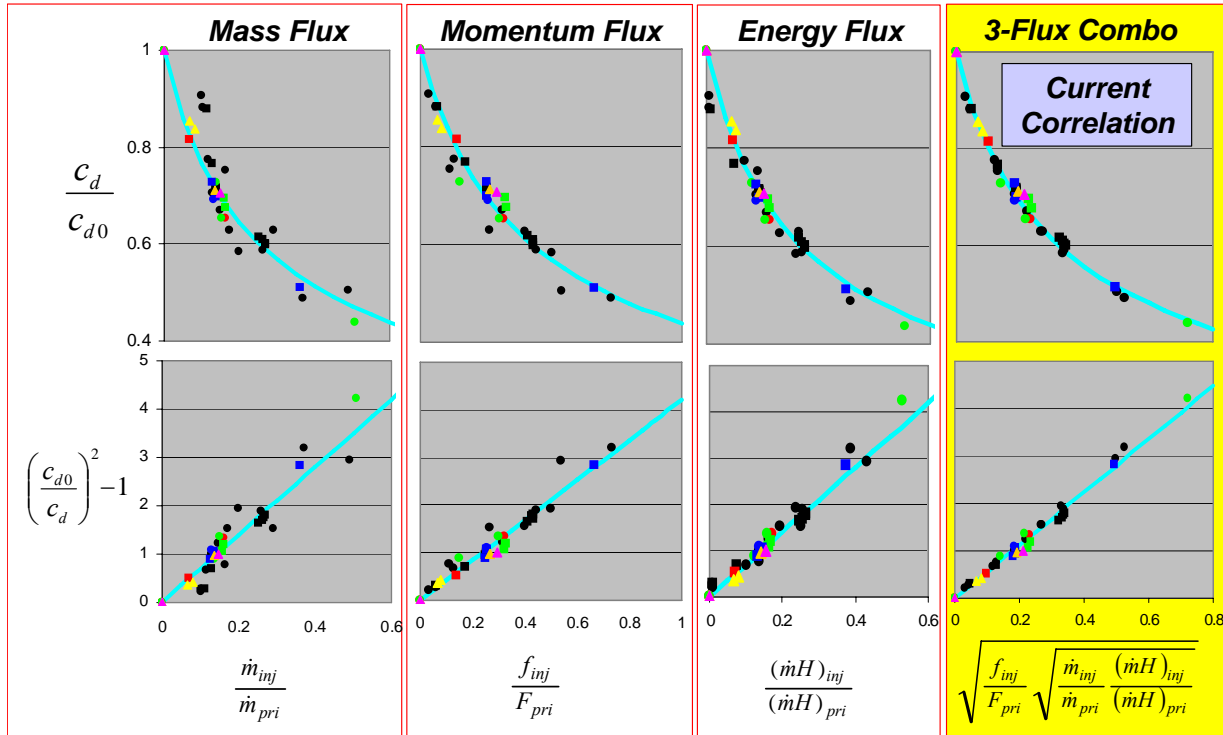


Figure 4. Comparison of discharge coefficient with various fluxes

Figure 5 compares the PIRFCT correlation and data with two polynomial correlations whose independent variables have been converted from $\frac{f}{F}$ to the combined flux function. The polynomial correlations were based upon steady injection with a similar injector configuration. The two polynomial correlations match the PIRFCT correlation well for low amounts of blockage ($\frac{C_d}{C_{d0}} > 0.7$), which is the range for which they were intended. However, PIRFCT required simulation of blockages in excess of 50%. The equivalent steady flux method and the combined flux function allow the PIRFCT correlation to apply to steady and pulsing cases over a large range of

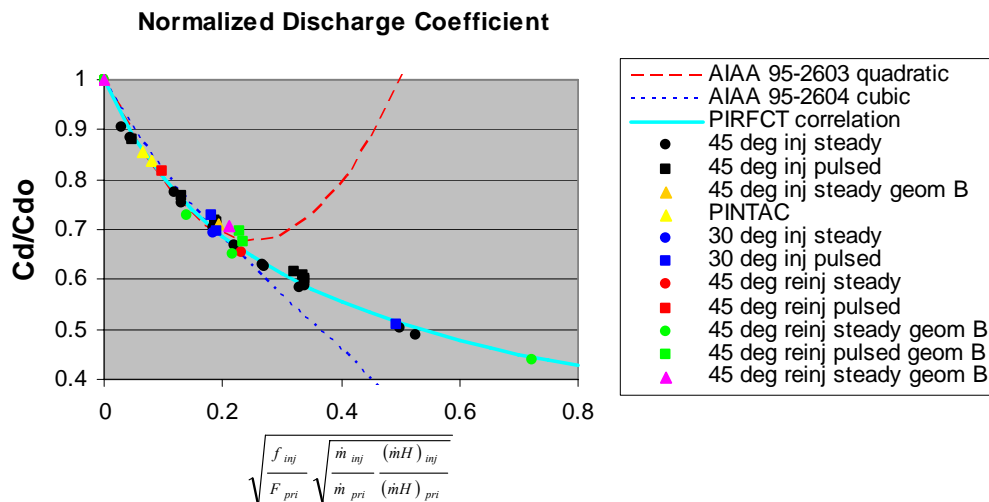


Figure 5. Discharge coefficient plotted against the combined flux function

throttling in this investigation.

These formulas and correlations indicate that c_d depends strongly upon $\omega\sqrt{\tau}$, but a weakly upon $\frac{P_{inj}}{P_{pri}}$ and M_{inj} , especially when $P_{inj} > P_{ref}$. Since high $\frac{P_{inj}}{P_{pri}}$ injection is generally expensive to achieve with hardware, the challenge is to develop a technique for injecting flow with low $\frac{P_{inj}}{P_{pri}}$ into the primary throat.

V. Multiple Injection Streams

A. Tertiary Flow

Injecting a stream with a low $\frac{P_{inj}}{P_{pri}}$ (≈ 1) at an angle which opposes the primary flow is difficult because the effective back pressure of the injector is fairly high relative to its source pressure. This prevents the injected flow from choking and significantly reduces mass flow. An injector with $\frac{P_{inj}}{P_{pri}} \approx 1$ would flow more mass if the back pressure could be reduced in the vicinity of the injector orifice. This is precisely what happens immediately downstream of a high-pressure injector. An additional injector placed in this region could exploit this low back pressure, thereby increasing its flow rate. Figure 6 shows a multiple injector design concept with a high pressure (secondary) injector immediately upstream of a low pressure (tertiary) injector. The secondary injector creates an environment which improves the flow rate (therefore ω) of the tertiary flow.

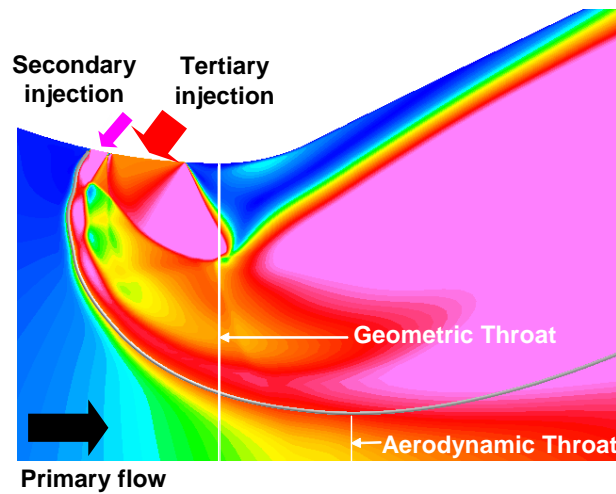


Figure 6. Secondary Injection of high pressure combined with Tertiary Injection of Low pressure

The equivalent steady concept is valid for multiple injection streams (pulsing, steady or a combination), because the nature of fluxes allows “like” fluxes to be summed. For example, for a case with multiple injection jets, the time-averaged mass flux from each jet may be summed to obtain a single equivalent steady mass flux. The momentum flux and energy flux may be summed in a similar manner. The independent variable, “ x ,” in the combined flux function may be expressed for multiple injection streams as follows:

$$x = \sqrt{\frac{\sum f}{F}} \sqrt{\frac{\sum \dot{m}_{inj}}{\dot{m}_{pri}} \frac{\sum (\dot{m}H)_{inj}}{(\dot{m}H)_{pri}}} \quad \text{where the summations are over each time-averaged injected flux.}$$

Time accurate simulations were performed on certain key cases to confirm the relationship with the equivalent steady case.

B. Assisted Reinjection

The tertiary injection described above is based upon the concept of its predecessor, assisted reinjection, which is pictured in figure 7. Reinjection diverts primary flow from a location upstream of the throat, and reintroduces it near the throat. The “assistance” is provided by a high pressure injector located immediately upstream of the reinjection point (Miller et al., 1997). The “reinjecting” flow has a low pressure ratio ($\frac{P_{inj}}{P_{pri}} \approx 1$) because it is bypassed from the primary stream. Therefore, a high pressure secondary injector provides the local low-pressure environment to improve effectiveness of reinjection, similar to the technique described for tertiary injection.

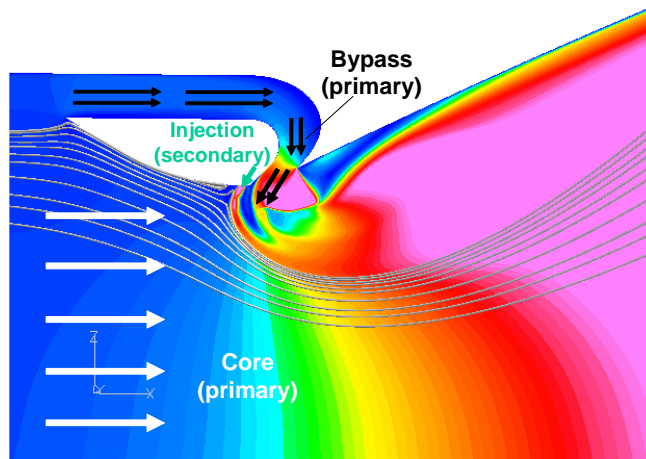


Figure 7. Assisted reinjection bypasses and reintroduces primary flow to provide blockage

The PIRFCT correlation was found to apply to assisted reinjection when the bypassed flow is bookkept in a manner which requires further defining the primary flow into “core” and “bypass” flow, and accounting for them in the correlation. As the names indicate, “bypass” refers to the flow which is bled off of the primary path, and reinjected. The “core” flow is the remaining primary flow downstream of the bypass. C_{d_0} is measured as the discharge coefficient when the “assistance” is removed (i.e., no secondary flow), and the reinjection is present. The combined flux function is expanded as:

$$x = \sqrt{\frac{f_{inj}}{F_{core+bypass}}} \sqrt{\frac{\dot{m}_{inj} (\dot{m}H)_{inj}}{\dot{m}_{core} (\dot{m}H)_{core}}}$$

Figure 8 shows a pulsed assisted reinjection case. Although the secondary flow is pulsed according to the modified “on” and “off” square wave, the reinjected flow (from the bypass) flows at a much more constant rate. Figure 8 shows the deep penetration of the vortices caused by the interaction between the pulsed and reinjected flows. However, this dramatic penetration is not accompanied by dramatic blockage. Recall that the bypassed flow is bookkept as primary flow in this study. Therefore primary flow is present inside and outside of the injected flow.

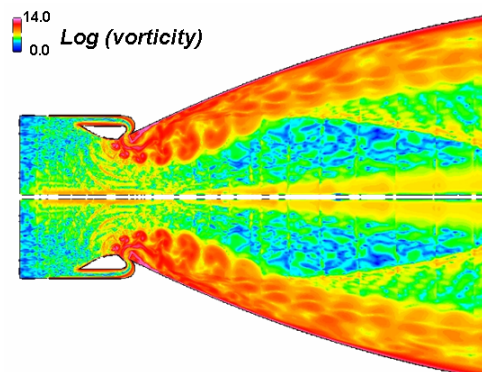


Figure 8. Pulsed Assisted reinjection shows dramatic penetration of vortices

The assisted reinjection concept was studied briefly, but it was soon modified into the tertiary flow concept in order to allow more control over the various streams, simplify the anticipated hardware issues, and remove the confusing bookkeeping of the bypass flow.

VI. The Benefit of Pulsing

The simulations indicate that the time-averaged amount of blockage (throttling) created by pulsed injection is approximated by simulating the equivalent steady case. The pulsed cases correlated so closely with the steady cases that the final correlation does not contain an additional variable to account for frequency. The “equivalent steady” approach is sufficient for capturing the effect of pulsing for this numerical study. This does not mean that the benefit of pulsing is non-existent. The benefit is simply estimated through the equivalent steady approach. Other pulsed-to-steady comparison methods based only upon mass flux could bias the results in favor of the pulsed case. For instance, investigators often perform comparisons by considering a steady jet, and then adding pulsing capability by pressurizing and pulsing the injected flow without enlarging the jet orifice. The average pulsed mass flow is matched with the initial steady case by either increasing the velocity and/or density during each pulse, essentially doubling the instantaneous mass flow during “pulse on” (for 50% duty cycle) and dropping it to zero during “pulse off.” The flux formulations shown previously indicate that this approach reproduces the mass flow of the initial reference steady case, but it increases the time-averaged momentum and energy flux. The results of this study indicate that the improvement in throttling capability may be attributed entirely to the increase in the time-averaged injected momentum and energy. The same throttling capability could have been achieved through steadily injecting the time-averaged fluxes of the equivalent steady case, which has higher momentum and energy fluxes than the initial reference steady case mentioned here. Note that these equivalent steady fluxes may be quite high, therefore impractical or impossible to achieve with an actual steady jet. However, pulsing offers a method of achieving them.

Another benefit of pulsing becomes apparent when one considers an extremely low frequency case (square wave, 50% duty cycle) where the solution has time to settle into a steady state during the pulse “on” phase, and then into another steady state during the pulse “off” phase. If the transition time between these states is negligible compared to the overall cycle time, then one could argue that the time-averaged c_d is simply the average of the pulse “off” (baseline) value and the pulse “on” value. This “two-state average” method predicts less blockage than the “equivalent steady” method predicts. By using the combined flux function and the PIRFCT correlation, the two estimates are shown below. Note that “ x ” represents the combined flux function for the equivalent steady (time-averaged) condition. Therefore, “ $2x$ ” represents the instantaneous combined flux function during the pulse “on” phase of the 2-state average:

$$\text{Equivalent Steady : } c_d = \frac{c_{d_0}}{\sqrt{1 + ax}}$$

$$\text{2 - State Average : } c_d = \frac{1}{2} \left(c_{d_0} + \frac{c_{d_0}}{\sqrt{1 + 2ax}} \right)$$

Figure 9 plots and compares the two methods for this hypothetical case (with a representative value of the constant “ a ”). The equivalent steady approach always predicts more blockage than the 2-state average. A case with such a low frequency was not simulated in PIRFCT. In this study, lower frequency pulsing caused the pressure waves which traveled forward toward the inflow boundary to strengthen. These waves subsequently caused the primary flow to undergo large fluctuations such that it appeared to approach resonance and underwent transient extremes which temporarily exceeded those of the pulse “on” and pulse “off” conditions. Nevertheless, a sufficiently low frequency is expected to be devoid of the strong wave interactions and behave in the manner described.

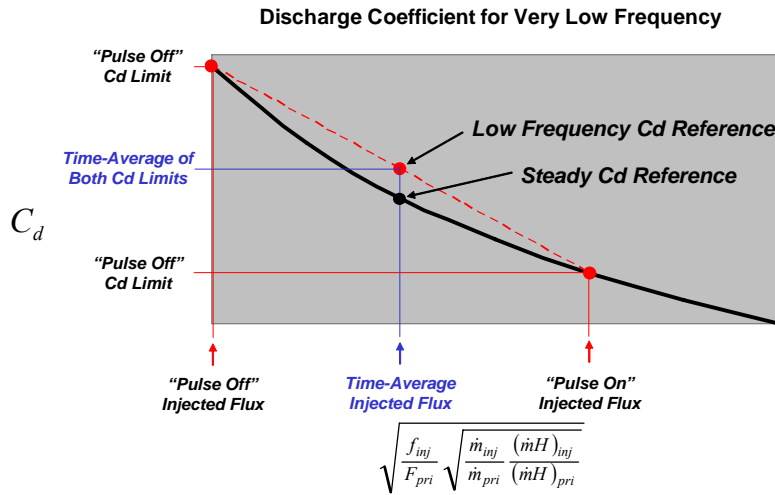


Figure 9. Equivalent steady injection predicts more blockage than average of “on” and “off” states

The pulsing frequencies in this study span a significant range, but all are high enough such that each injected pulse interacts with the previous pulse. That is, each pulse translates downstream a short distance (of the order of the injection slot width) before the next pulse emerges. The 2-state average approach would probably require a frequency several orders of magnitude lower.

Close inspection of the CFD results reveals that the lower frequency pulsing tends to have slightly less blockage (worse throttling performance) than a higher frequency and/or the equivalent steady case. Because the effect was small among the simulations, the frequency was not included in the correlation, but the investigators noticed that an artifact of highest (best) blockage was a sustained quasi-steady separation standing at the downstream edge of the jet. If the frequency dropped such that this separation disappeared between pulses, then the time-averaged blockage was noticeably less than the equivalent steady case. This behavior was not examined in detail, but it is suspected to be caused by allowing the primary flow to reattach during the time between pulses (pulse “off”). If this “off” time is too low to allow reattachment, then the pulsed injection better mimics the equivalent steady case. This behavior is expected to depend upon frequency as well as duty cycle. Figure 10 shows the position of the separation relative to the injector.

Another contributor to the decreased performance could be the effective change in geometry due to the area of the injection jet. When this orifice area becomes significant, then changing it by a factor of two (to compare steady and 50% duty-cycle pulsed cases) could change the distribution of the injected flow such that the primary flow conditions at the injector are characterized by a range of values, rather than a single value. That is, a large-area injector is no longer a point source.

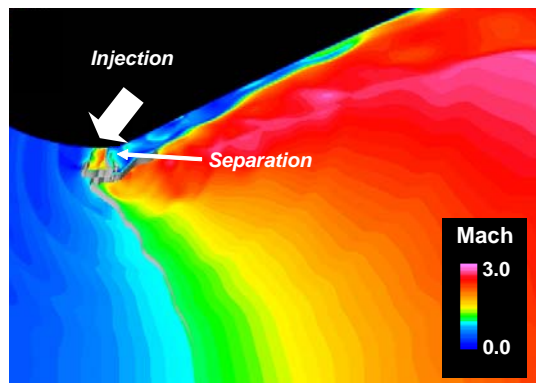


Figure 10. Best pulsing blockage is accompanied by a sustained separation aft of injector.

VII. Exit Thrust

The streamtube containing the injected flow occupies a finite volume along the nozzle. This streamtube reduces the effective nozzle exit area of the primary flow, thereby reducing the gain in expansion ratio provided by flow control at the throat. However, the injected flow contributes significant thrust, which offsets the decrement due to blocked exit area. The ideal thrust (assuming zero back pressure) is approximated from the stagnation conditions and mass flow of the primary and injected flows, and the assumption that the streamtubes (each of which is an ideal gas) expand such that the pressures equalize and the areas sum to fill the nozzle exit.

Figure 11 compares the Vacuum Specific Impulse, I_{sp} , of several cases with the isentropic limit. I_{sp} is calculated as the total exit thrust divided by the sum of the mass flows (primary plus all injected flows). The contribution from any injected flow tends to be higher when the injected flow temperature is high. Although significant P_t losses occur within the injected streamtubes due to turning and shear, the overall vacuum I_{sp} is within about 3% of the ideal value. Only a cursory look at the thrust was conducted because many of the CFD grids were built for focusing upon the solution in the vicinity of the injector rather than the exit. A formal study of the exit solution would warrant building grids with more detail throughout the length of the nozzle. However, the preliminary results indicate that the isentropic thrust limit is a rough indicator of the simulated performance.

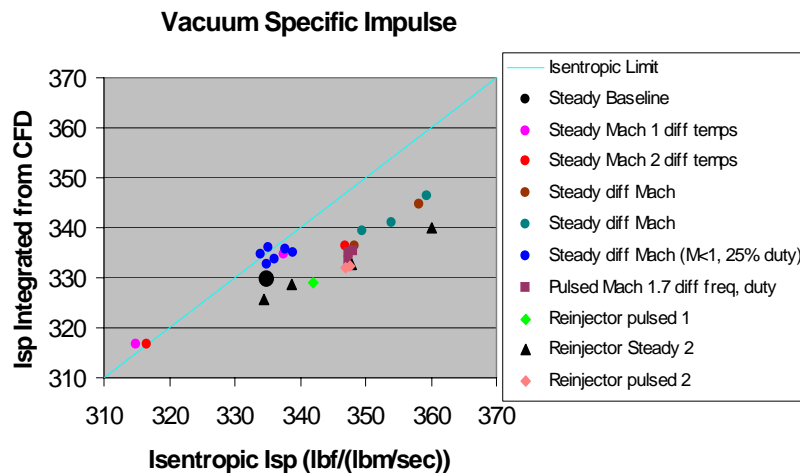


Figure 11. Vacuum Specific Impulse compares with isentropic limit for injection cases.

Fluidic injection modifies the effective aerodynamic contour of the nozzle. The intention in this study is to use injection to create an aerodynamic throat for throttle control. However, a side effect is a change in the effective shape of the divergent part of the nozzle. Figure 12 shows Schlieren-like images of a nozzle configured with steady and pulsed injection. The steady case shows a shock which emanates from an aerodynamic concave corner caused by injection. The pulsing counterpart contains a similar shock standing fairly steadily while the injected pulses convect downstream. These shocks are absent (or much weaker) when injection is removed. Other studies show that small imbalances in nozzle shocks could lead to substantial side forces (thrust vectoring). Therefore, the physical geometry could be redesigned as necessary to control or reduce the consequences of these shocks when flow control is active.

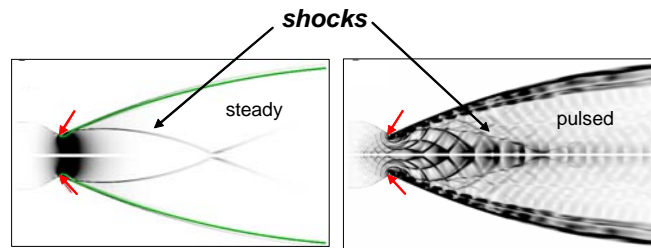


Figure 12. Shocks stand in the divergent section of a nozzle with steady and pulsed fluidic injection

VIII. Conclusion

During the PIRFCT program, insight was gained into the physics of pulsed injection for the throttling of supersonic nozzles. A general correlation was developed which estimates the throttling effect of forward directed injection near the throat. The effect of pulsing was found to be quantifiable in terms of the time-averaged fluxes of mass, momentum and energy. However, the system trade study performed on the rocket application of an earth-to-orbit mission concluded that the thrust benefit of flow control, which was hoped to allow higher payloads, was nearly canceled by the estimated weight penalty of the injection hardware and the thrust losses predicted when the PIRFCT system was active. Future advances in technology which reduces the weight of injection hardware could tip the results in favor of flow control. However, a more promising application may be an aerospace vehicle with a larger portion of its trajectory spent at lower altitudes where changes in back pressure are more significant. Therefore, a follow-on program is now underway for a different application.

IX. Acknowledgments

This research was funded by the Defense Advanced Research Projects Agency (DARPA) and managed by the Air Force Research Laboratory (AFRL). Their support and insight is greatly appreciated.

X. References

1. Anderson, John D. Jr., "Modern Compressible Flow with Historical Perspective," 1982, McGraw Hill, pp 195-200.
2. Bender, E., Miller, D., Smith, B., Yagle, P., Vermeulen, P., Walker, S., 2000, "Simulation of Pulsed Injection in a Crossflow Using 3-D Unsteady CFD," AIAA No. 2000-2318.
3. Catt, J.A., Miller, D.N. and Giuliano, V.J., "A Static Investigation of Fixed-Geometry Nozzles Using Fluidic Injection for Throat Area Control," AIAA, Paper No. AIAA 95-2604
4. Miller, D., Yagle, P., Hamstra, J., 1999, "Fluidic Throat Skewing for Thrust Vectoring in Fixed-Geometry Nozzles," AIAA, Paper No. 99-0365.
5. Miller, D.N. and Catt J.A., 1995, "Conceptual Dev. of Fixed-Geometry Nozzles Using Fluidic Throat-Area Control," AIAA, Paper No. 95-2603.
6. Miller, D.N., Catt J.A., and Walker, S.H., 1997, "Extending Flow Control of Fixed Nozzles Through Systematic Design: Introducing Assisted Reinjection," ASME, Paper No. FEDSM97-3680.
7. Miller, D.N., Yagle, P.J., Bender, E.E., Smith, B.R., 2001, "A Computational Investigation of Pulsed Injection into a Confined, Expanding Crossflow," AIAA 2001-3026.
8. Rizzeta, D.P., Visbal, M.R. and Stanek, M.J., 1998, "Numerical Investigation of Synthetic Jet Flowfields," AIAA Paper No. 98-2910.
9. Roe, P.L., 1981, "Approximate Riemann Solvers," J. of Comp. Physics, Vol. 43, pp. 357-372.
10. Roe, P.L., 1981, "Some Contributions to the Modeling of Discontinuous Flows," Proceedings of the SIAM/SMS Seminar.
11. Smagorinsky, J., 1963, "General Circulation Experiments with the Primitive Equations," Mon. Weather Rev., Vol. 91, pp. 99-164.

12. Smith, B.R., "The k-kl Turbulence Model and Wall Layer Model for Compressible Flows," AIAA 90-1483.
13. Stone, H.L., 1968, "Iterative Solution of Implicit Approximations of Multidimensional Partial Differential Equations," *SIAM J. of Numer. Anal.*, Vol. 5 1968, pp. 530-538.
14. Sweby, P.K., 1984, "High Resolution Schemes Using Flux Limiters for Hyperbolic Conservation Laws," *SIAM J. Numer. Anal.*, Vol. 21, pp. 995-1101.
15. Vakili, A., Sauerwein, S., Miller, D., 1999, "Pulsed Injection Applied to Nozzle Internal Flow Control," AIAA No. 99-1002.
16. Vakili, A.D., Chang, Y.K. and Wu, J.M., 1991, "Vortex Rings in Uniform Crossflow," AIAA, Paper No. 91-0522.
17. Van Leer, B., 1976, "MUSCL, a New Approach to Numerical Gas Dynamics," *Computing in Plasma Physics and Astrophysics*, Germany, April, 1976.
18. Vermeulen, P., Ramesh, V., Miller, D., Yagle, P., Bender, E., "Ejector Pumping Effectiveness Through Pulsing Primary Flow," ASME, Paper GT-2002-30007.
19. Vermeulen, P., Ramesh, V., Meng, G., Miller, D., and Domel, N., 2004, "Air Ejector Pumping Enhancement Through Pulsing Primary Flow," AIAA 2004-2621.
20. Vermeulen, P., Ramesh, V., Meng, G., Miller, D., and Domel, N., 2004, "Ejector Enhancement Through Pulsing Primary Flow," Final Report, AFOSR Grant No. F49620-02-1-0131.
21. Walker, S., 1997, "Lessons Learned in the Development of a National Program," AIAA 97-334.
22. White, Frank Mangrem, "Viscous Fluid Flow," 1974, McGraw Hill, Inc., pp. 143-145.
23. Wing, D.J., 1994, "Static Investigation of Two Fluidic Thrust-Vectoring Concepts on a Two-Dimensional C-D Nozzle," NASA TM 4574.
24. Yagle, P., Miller, D., Ginn, K., Hamstra, J., 2000, "Demonstration of Fluidic Throat Skewing for Thrust Vectoring in Structurally Fixed Nozzles," ASME No. 2000-GT-0013.
25. Yagle, P., Miller, D., Bender, E., and Smith, B., 2002, "A Computational Investigation of Pulsed Ejection," AIAA 2002-3278.